A Salt-Bridge Motif Involved in Ligand Binding and Large-Scale Domain Motions of the Maltose-Binding Protein

Thomas Stockner, Hans J. Vogel, and D. Peter Tieleman
Department of Biological Sciences, University of Calgary, Calgary, Alberta, Canada

ABSTRACT The uptake of nutrients is essential for the survival of bacterial cells. Many specialized systems have evolved, such as the maltose-dependent ABC transport system that transfers oligosaccharides through the cytoplasmic membrane. The maltose/maltodextrin-binding protein (MBP) serves as an initial high-affinity binding component in the periplasm that delivers the bound sugar into the cognate ABC transporter $MalFGK_2$. We have investigated the domain motions induced by the binding of the ligand maltotriose into the binding cleft using molecular dynamics simulations. We find that MBP is predominantly in the open state without ligand and in the closed state with ligand bound. Oligosaccharide binding induces a closure motion (30.0° rotation), whereas ligand removal leads to domain opening (32.6° rotation) around a well-defined hinge affecting key areas relevant for chemotaxis and transport. Our simulations suggest that a "hook-and-eye" motif is involved in the binding. A salt bridge between Glu-111 and Lys-15 forms that effectively locks the protein-ligand complex in a semiclosed conformation inhibiting any further opening and promoting complete closure. This previously unrecognized feature seems to secure the ligand in the binding site and keeps MBP in the closed conformation and suggests a role in the initial steps of substrate transport.

INTRODUCTION

Periplasmic-binding proteins serve as primary high-affinity receptors for active transport of various nutrients across the inner membrane of Gram-negative bacteria (1,2); ~100 family members are known, and they specifically bind substrates as varied as amino acids, carbohydrates, oxyanions, polyamines, and vitamins (3–5). They share a common structural fold consisting of two lobes of similar size (6,7). The conformation of these lobes each shows a Rossman fold or α/β motif that is composed of a β-sheet core flanked on both sides by α-helices. Conformational changes involving a reorientation of these lobes play a key role in the ability of the periplasmic binding proteins to capture their respective substrates (8).

The maltose-binding protein (MBP) belongs to the maltose transport system, an ATP-binding cassette (ABC) transporter (9,10) that accumulates linear maltooligosaccharides of up to seven α(1–4) linked glucose units (11,12). It can increase the maltose concentration 10^5-fold against the concentration gradient (13). The maltose transporter depends on the periplasmic MBP for transport, but MBP-independent mutants of the integral membrane proteins MalF and MalG have been identified (14). Allele-specific suppressor MBP mutants, e.g., Gly-13Asp, Asp-14Tyr, or Tyr-210Asp, can restore MBP-dependent transport to these $MalFGK_2$ mutants (15), whereas suppressing wild-type transporters (16). The first crystal structures of MBP were solved by Sharff et al. (8) in the open conformation and by Spurlino et al. (6) in the closed conformation, highlighting a large conformational hinge bending motion (>30° rotation) upon ligand binding. The maltose-binding protein binds maltooligosaccharides in the deep groove between the N- and the C-terminal domain. Maltotriose has the highest binding affinity ($K_d \sim 1.6 \times 10^{-7}$ M), other maltooligosaccharides bind one order of magnitude less strongly (11), whereas glucose, the basic monosaccharide unit, does not bind.

We have used molecular dynamics (MD) simulations to study the sequence of events involved in the large-scale conformational changes that occur during the transition that follows maltotriose binding or release. In simulations of the structurally related proteins glutamine-binding protein (17) and the ligand-binding domain of the glutamate receptor (18), no complete transition could be detected on the shorter timescale of these studies; however, the presence of the expected conformational changes was indicated by extensive mobility in their directions. Substantial energy barriers can impede simulations of the complete transition pathway (19,20). Normal mode analysis (21–23) allows the prediction of conformational changes from a single crystal structure and does not require the high computational cost of MD, but this approach has its own limitations. The transition can be directly estimated, if crystal structures are available in more than one conformation (24), but the picture is based on only the most stable open and closed states captured in the crystal structure, whereas mechanistically important interactions along the interconversion pathway might remain hidden.

We are interested in the mechanism of substrate binding with a focus on the structural changes that can occur in periplasmic binding proteins (5). Here we report converged MD simulations of the functionally important transition between

Submitted June 27, 2005, and accepted for publication August 26, 2005.

Address reprint requests to D. Peter Tieleman, Dept. of Biological Sciences, University of Calgary, 2500 University Dr. NW, Calgary, Alberta T2N 1N4, Canada. Tel.: 403-220-2966; Fax: 403-289-9311; E-mail: tieleman@ucalgary.ca.

0006-3495/05/11/3362/10 $2.00

doi: 10.1529/biophysj.105.069443

the open and the closed state of MBP as the fast substrate binding (association constant of 2.5×10^{-7} $M^{-1}s^{-1}$) (25) allows for a direct investigation by MD simulations, which were performed without any bias or guidance and the structural changes are solely due to changes in the ligand-binding state. The combination of simulations, starting from different conformations and ligand-binding states, allows us to investigate the structural transitions in both directions and to estimate convergence. We focus on the sequence of events on a local and a global scale. Our analyses show that the domain closure is not a completely linear motion: an intermediate structure displays a correlated sequence of conformational changes, which we characterize as a hook-and-eye motif. This mechanism secures the ligand in the binding site and locks MBP in a closed conformation.

MATERIALS AND METHODS

The crystal structures of MBP (370 residues) with the Protein Data Bank entry codes 1LLS (open apo structure) (26) and 3MBP (closed holo structure) (11) were obtained from the Protein Data Bank. The structures were carefully checked using the server Biotech Validation Suite for Protein Structures (27); the side chains of some Gln, Asn, and His residues needed to be inverted to have the correct orientation for hydrogen bonding. Four simulations were carried out. Two simulations started from the open conformations, in the absence and presence of ligand (apo-reference and holo-transition, respectively) and two simulations started from the closed conformation, with and without ligand (holo-reference and apo-transition, respectively). The open holo-transition starting structure was constructed by extracting the coordinates of the sugar residue from the ligand-bound 1EZ9 (28) crystal structure and inserting the sugar into the open structure (1LLS) after fitting the backbone atoms of the C-terminal domain of both structures. The linear sugar unit at the reducing end of the sugar chain as present in the 1EZ9 structure was removed. The binding site of the remaining three sugar units coincides with the positions occupied in the closed holo structure, binding site S1 to S3. The MBP structures were solvated with water in a truncated dodecahedron water box with a minimal distance to the box wall of 1 nm for the protein in the most open conformation. The initial box size was the same in all simulations. The water was equilibrated and eight sodium ions were added to neutralize the system. The protein was slowly released by reducing the restraining force on all protein atoms (1000, 100, 10, 1, 0 kJ/mol nm^2) in five steps (20 ps each).

MD simulations were carried out using the GROMACS 3.0 MD package (29,30). The protein and the maltotriose were represented using the GROMOS96 43a2 force field (31), with SPC water (32). The simulations were carried out for 30 ns with a constant temperature of 300 K, using a Berendsen ($\tau_T = 0.1$ ps) thermostat (33), while coupling the protein, the maltotriose, and the water/ions separately. The pressure was maintained at 1 bar using the weak coupling algorithm (33) with a coupling constant of 1.0 ps and a compressibility of 4.6×10^{-5} bar^{-1}. The electrostatic interactions were evaluated using the smooth particle mesh Ewald method (34,35), with a cutoff of 0.8 nm. The long-range electrostatic interactions were calculated with sixth-order B-spline interpolation and a Fourier spacing of 0.12 nm. The Lennard-Jones interactions were evaluated using a twin-range cutoff (0.8 and 1.4 nm) with the neighbor list updated every three steps. All bonds in the protein and ligand were constrained using LINCS (36). The bonds and the angles of the water molecules were constrained using the SETTLE algorithm (37). Additionally, the hydrogen atoms of the protein were treated as dummy atoms (38) allowing a time step of 5 fs.

The trajectories are analyzed in terms of essential dynamics analysis (39), which is based on the diagonalization of the covariance matrix of atomic fluctuations. The 2-D projection is calculated by the inner product between actual atomic coordinates and the direction of the eigenvector. Additionally we calculate the inner product between eigenvectors to compare the motion displayed in different simulations.

The distance distribution function $P(r)$ is calculated as an atom pair distribution and is normalized to one using a bin-width of 0.05 nm and averaging over the last 10 ns of the trajectory.

The domain motion analysis was done using DynDom (40,41). The standard ratio of 1 is used to distinguish between interdomains and intradomain motions. A window length of 9 residues was used together with a minimal domain size of 11 residues.

RESULTS

The MBP has been crystallized in the open (1LLS) and the closed conformation (3MBP) and the structures differ by a 36.9° rotation of the N-terminal domain relative to the C-terminal domain. We investigated the conformational changes induced by ligand binding or ligand removal and obtained a global picture based on four simulations of the open and closed MBP conformations in the holo (ligand-bound) and the apo (ligand-free) state. The evolution of the radius of gyration (R_g) and the domain opening angle θ (defined as the angle between the centers of mass of the N-terminal domain, the central hinge β-sheet and the C-terminal domain) clearly indicates large structural changes (Fig. 1, *A* and *B*). We include the sugar ligand in the calculation of the R_g of both holo simulations (holo-reference and holo-transition) for a better comparison with experimental values. The results show that the θ and R_g are relatively stable in the closed holo-reference and the open apo-reference simulations. Large changes occur in the simulations starting from the modified structures (apo-transition and holo-transition). The holo-transition simulation shows a closure motion burying the substrate in the binding cleft. The transition is clearly visible in Fig. 1, where R_g and θ simultaneously decrease. Removal of the ligand (apo-transition) from the closed structure induces domain opening. The R_g and θ rise toward values reflecting the open structure. Interestingly, we notice an initial drop of the R_g in all simulations. The R_g recovers in the holo simulations but in the apo-reference simulations continues to decrease and remains significantly below the value derived from the crystal structure (R_g, averaged over the last 10 ns; apo-reference: 2.119 ± 0.013 nm, apo-transition: 2.162 ± 0.010 nm, holo-transition: 2.062 ± 0.008 nm, and holo-reference: 2.057 ± 0.008 nm). These calculated R_g values are consistently smaller than the experimental values (42) (apo: 2.198 ± 0.010 nm, maltose-bound: 2.095 ± 0.011 nm, maltotriose-bound: 2.066 ± 0.007 nm). The experimental R_g of maltotriose-bound MBP seems to be very low. Small differences of the radius of gyration (2–4%) and the molecular dimension can originate from the first hydration shell (0.3-nm thickness) surrounding the protein (43) that has a significantly higher density (10–20%) than bulk water (44).

The domains behave largely like rigid bodies, remaining very stable and close to the initial conformation even

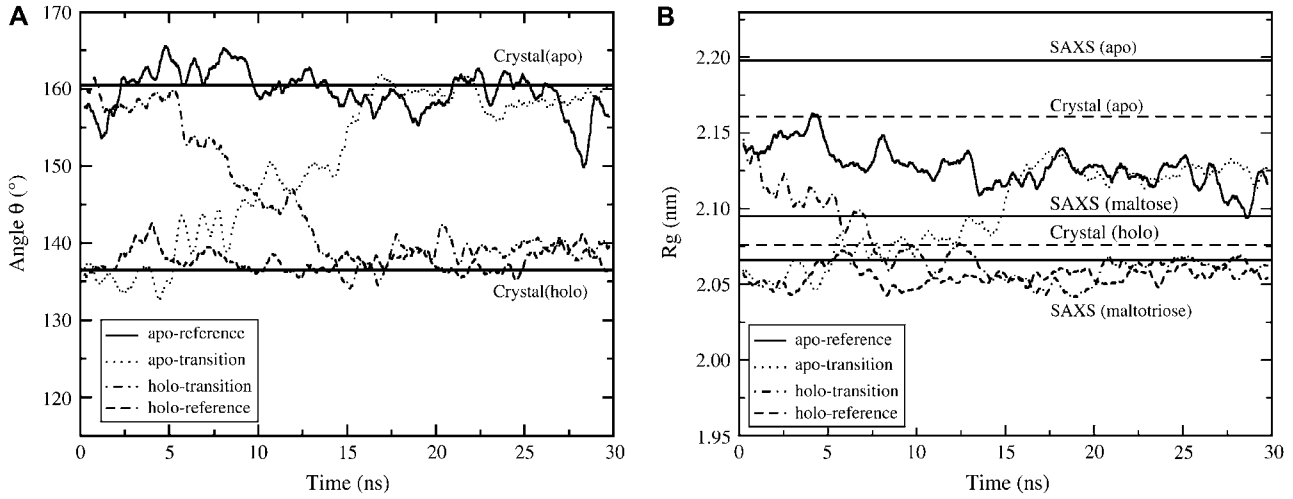

FIGURE 1 (*A*) Domain opening angle θ, defined as the centers of mass (Cα atoms) of the N-terminal domain (residues 1–108, 263–311), the central β-sheet hinge residues (109–112, 259–262), and the C-terminal domain (113–258, 320–370). The horizontal lines represent the values for the crystal structures (apo form and holo form). (*B*) The radius of gyration (R_g). All protein atoms are included in the analysis. The maltotriose ligand is included in the analyses of the holo simulations to allow for a direct comparison with experiments. The horizontal lines represent starting structures and experimental values from SAXS. Data points have been smoothed using a 50 data point window.

during significant changes of their relative orientation. We monitored the root mean-square deviation (rmsd) of the N-terminal (residue 1–108, and residue 263–311) and the C-terminal domain (residue 113–258 and residue 320–370) individually and determined their stability (see *insets* of Fig. 2). The rmsd values reach a comparable level of 0.15–0.20 nm in all simulations. No significant differences exist between the apo and the holo simulations, indicating that the structures of the individual domains remain largely unperturbed on the simulation timescale.

Changes in the time-dependent rmsd of the Cα atoms (residues 5–369) correlate with the behavior of θ and R_g. The rmsd (see Fig. 2) rises to normal levels of ~0.2–0.3 nm in the reference simulations. The holo-transition simulation, starting from the open conformation, shows a large increase of the rmsd values relative to the open starting structures (Fig. 2 *A*), reflecting the transition away from the open state. Comparing the same trajectory with the closed crystal structure (Fig. 2 *B*) shows an initially large rmsd (~0.4 nm) that decreases to the value of the holo-reference simulation (0.18 nm). The identical, but opposite transition occurs upon removing the ligand from the closed conformation (apo-transition).

In addition to R_g we can calculate the distance distribution function $P(r)$. Comparing our calculated $P(r)$ function

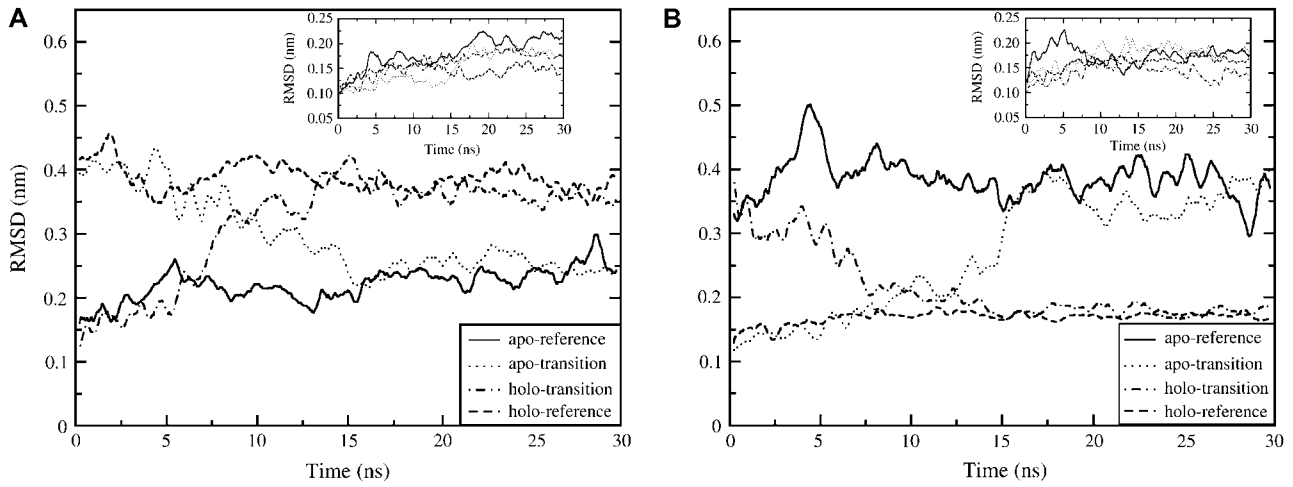

FIGURE 2 Time evolution of the rmsd of the Cα atoms for the four simulations. (*A*) The rmsd values with respect to the open apo crystal structure. (*B*) The rmsd values with respect to the closed holo crystal structure. The insets show the structural stability of each domain individually: the rmsd of the Cα atoms from the starting structure of the N-terminal domain is shown in the inset of panel *A* and for the C-terminal domain in the inset of panel *B*. The analyses exclude the flexible terminal residues 1–5 and 369–370. Data have been smoothed using a 50 data point window.

(averaged over the last 10 ns), shown in Fig. 3, with the $P(r)$ function determined by small angle x-ray scattering (SAXS) measurements (42) shows that the properties are very similar. The shapes coincide, the ligand-bound MBP is smaller than the ligand-free MBP and the molecule dimensions are similar. The maximal molecular size determined from our simulations, truncating the $P(r)$ function at 1% of its maximal values, is 6.0 nm (holo-transition) and 6.2 nm (holo-reference) for the close holo state and 6.4 nm for both apo MBP simulations.

We analyzed the nature of the structural changes (holo-transition and apo-transition) using DynDom (40,41), by comparing the starting structures to the structures closest to the average conformation (averaged over the final 10 ns). Fig. 4 *A* shows the 30.0° rotation of the N-terminal domain of the holo-transition simulation by an overlay of the Cα atoms of the C-terminal domains. The screw axis is located close to the backbone atoms of the β-sheet that connects the two domains (residues Val-110, Glu-111, Val-259, Gly-260, Val-261) and the loop connecting helix XIII and helix XIV (Pro-315–Ala-319). The hinge residues are Val-110 to Ala-112, Val-259 to Val-261, and Asp-314 to Ala-319. The apo-transition simulation shows the transition in the opposite direction, starting from a closed structure and displaying a domain opening motion. Fig. 4 *B* highlights this 32.6° opening motion by showing the closed and open structure fitted to the Cα atoms of the C-terminal domain. The screw axis is again placed close to the hinge residues (Val-110, Glu-111, Gly-260, Val-261). The hinge is defined as Ala-109 to Ala-112, Gly-260 to Leu-262, and Arg-316 to Ile-317. In the crystal structure the β-hairpin (Lys-170 to Asp-177) is detached from the protein body, making crystal packing interactions with an adjacent MBP molecule in the asymmetric unit cell. In the simulations starting from the closed crystal structure (11) the β-hairpin relaxes and covers the exposed hydrophobic residues (Ile-178, Ile-329, Ile-333) beneath.

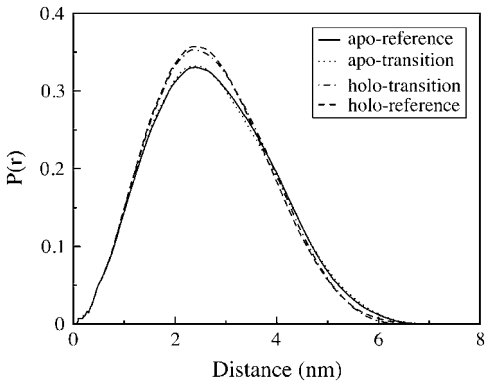

FIGURE 3 Distance distribution function $P(r)$. The coordinates of the heavy atoms are averaged over the last 10 ns. The ligand is included in the analysis in the holo trajectories. A bin width of 0.05 nm has been used.

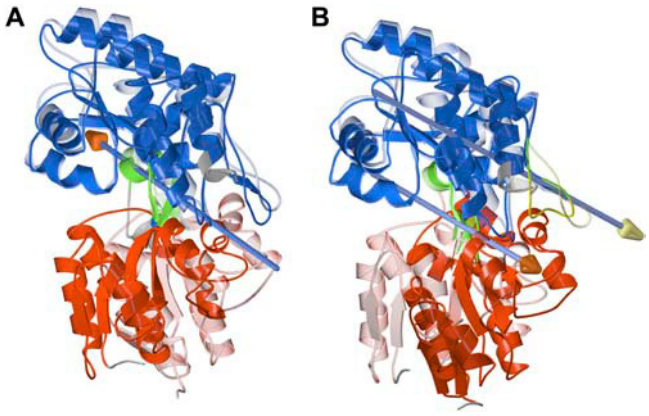

FIGURE 4 Domain motions: the starting structures are displayed in transparent mode together with the structure closest to the average over the stable final 10 ns. The N-terminal domain is shown in red, the C-terminal domain in blue, and the hinge region as identified by DynDom in green. The arrows represent the screw axes. (*A*) The domain closing motion of the holo-transition simulation. (*B*) The domain opening motion of the apo-transition simulation. A second conformational change (β-hairpin Lys-170 to Asp-177) is identified on the ''backside'' of the MBP. Figures are prepared with MolScript (67) and Raster3D (68).

The most important motions displayed in a trajectory can be investigated using essential dynamics analysis. The eigenvectors with the largest associated eigenvalues describe the most important motions (39), in our case the domain opening motion. The similarity between our 4 trajectories and the overlap of the sampled phase space is estimated by projecting all 4 simulations onto the same plane spanned by the first two eigenvectors of the apo-transition trajectory, shown in Fig. 5. The reference simulations holo-reference (*blue*) and apo-reference (*red*) sampled nonoverlapping regions of the configurational space and remain near their respective starting structures. A transition from one state to the other is evident in the two transition simulations. The holo-transition simulation (*yellow*) samples initially the area of the open MBP conformation. The conformation then shifts during the transition toward the closed state, populating a region that overlaps with the holo-reference simulation. The apo-transition simulation (*cyan*) displays a conformational change in the opposite direction. Initially, the trajectory resembles a closed conformation, followed by a transition toward the open state, whereas the final fully open state samples an area that partially overlaps with the open apo-reference simulation. The first eigenvector of each transition simulation (apo-transition and holo-transition) is strongly correlated with the opening/closure motion. The normalized cross correlation fluctuation coefficient between the projection of the trajectories along the first eigenvector and the respective time evolution of θ is 0.95 for the apo-transition simulation and 0.98 for the holo-transition simulation. The inner product of the first eigenvectors of these two trajectories is 0.73, confirming a strong similarity of the transition pathway.

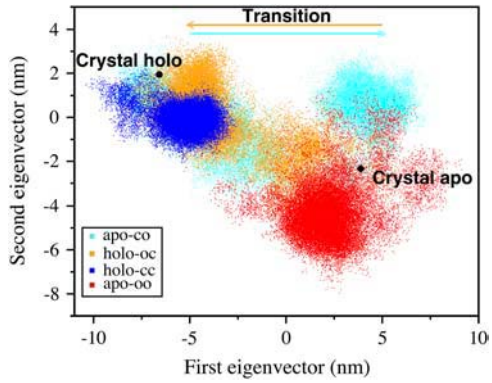

FIGURE 5 Projections of the protein backbone for all trajectories onto the first two eigenvectors of the apo-transition simulation, superimposed onto each other. The crystal structures are included to indicate the starting position of our simulations. The arrows indicate the direction of the transition.

The formation of a salt bridge between the side chains of Glu-111 in the hinge region and Lys-15 in the N-terminal domain triggers a series of highly correlated rearrangements as shown in Fig. 6 and Fig. 7. The maltotriose ligand is not shown for clarity. The initial hydrogen bond interactions involving Glu-111 (Fig. 6 *A*) changes to the new arrangement (Fig. 6 *B*) during the domain closure motion when the backbone carbonyl group of Glu-111 is pulled out of the β-sheet hydrogen bond formed with Gly-260 (Fig. 7 *A*) as its side chain forms a salt bridge with the side chain of Lys-15 (Fig. 7 *B*). The backbone carbonyl oxygen of Glu-111 forms a new hydrogen bond to the hydroxyl group of Tyr-155. Tyr-155 accepts an additional hydrogen bond from the NH group of Gly-260, effectively bridging the original β-sheet hydrogen bond. The backbone angles of Glu-111 and neighboring residues display sudden coordinate flips together with the formation of the Glu-111–Lys-15 salt bridge (Fig. 7 *D*). They move back to the previous state when the original β-sheet hydrogen bond with Gly-260 is restored and MBP assumes a completely closed conformation (Fig. 6 *C*). The salt bridge distance between Glu-111 and Lys-15 remains almost constant once formed whereas the cleft closes further.

DISCUSSION

MD simulations were used to investigate the most stable states of the apo and holo form of MBP, to follow the domain closure motion triggered by the addition of the maltotriose ligand as well as to study the domain opening induced by ligand removal from the closed structure. The transitions occur spontaneously upon changing the binding state. We reach convergence in the holo as well as in the apo simulations, indicated by rmsd, θ, R_g, and the overlap of the 2-D projection (see Figs. 1 and 5). The observed domain closure (30.0°) and opening (32.6°) are slightly smaller (see Fig. 1) than predicted by the crystal structures (36.9°). The average closed structure is moderately less closed, whereas the apo simulations converge to a slightly less open conformation. Our data indicate that the open state shows remarkable flexibility (θ varies between 144 and 168°), most probably because of the small number of interdomain interactions. The open MBP crystal structure adopts a very open conformation, possibly selected by crystal packing. The apo wild-type MBP crystal structures (1JW4 (28), 1LLS (26), 1OMP (8)) show minimal variability in their relative opening angles (159–160°). Similar large fluctuations have been found by Pang et al. (17) in simulations of the open apo glutamine-binding protein, although they could not observe a complete transition between states.

The crystal structures of the periplasmic siderophore-binding protein FhuD and the vitamin B_{12} binding protein BtuF have shown that there is a second class of periplasmic binding proteins that has a similar bilobal structure but contains a long α-helix connecting the two domains (45,46). These proteins do not undergo a large domain reorientation, when the ligands dissociate from the protein (47). Indeed, MD simulations of the FhuD protein with its ligand removed appear consistent with this restricted motion (48), as well as preliminary results obtained with the BtuF protein (C. Kandt, Z. T. Xu, T. Stockner, and D. P. Tieleman; unpublished results). It will be interesting to see how these proteins are recognized in a ligand-specific manner by their cognate transporter.

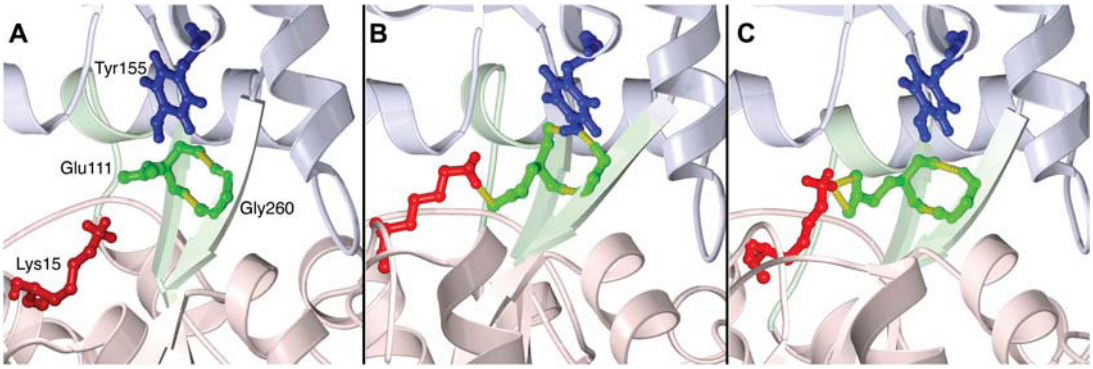

FIGURE 6 Hook-and-eye motif: representative structures (holo-transition simulation) of the (*A*) open, (*B*) intermediate, and (*C*) closed conformations, showing the hydrogen bond interactions (*yellow*) of Glu-111 with Lys-15, Tyr-155, and Gly-260. The sugar ligand is not shown for clarity.

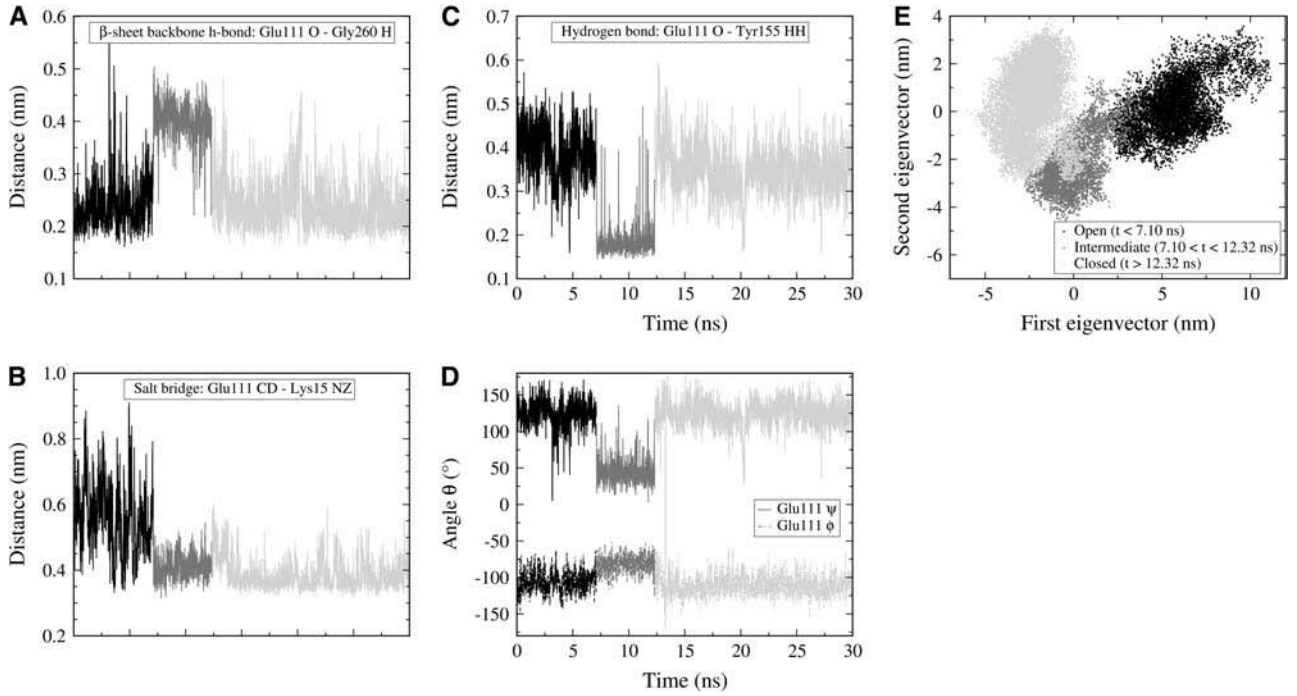

FIGURE 7 Changes in local interactions of the important residues Lys-15, Glu-111, Tyr-155, and Gly-260 in the holo-transition simulation. The color-coding represents the open conformation (*black*), an intermediate conformation (*dark gray*), and the closed conformation (*light gray*) with the time points defined by the change of the β-sheet hydrogen bond. (*A*) The disruption of the β-sheet hydrogen bond due to the salt bridge formation displayed in panel *B*. (*C*) The simultaneous formation of the hydrogen bond between Glu-111 and the hydroxyl group ring of Tyr-155. (*D*) The backbone ϕ- and ψ-angles of Glu-111. (*E*) The 2-D projection of the two largest eigenvectors of the holo-transition simulation.

The pathways of the conformational changes (opening and closing) overlap strongly. The similarity is evident in the domain rotation analysis. The screw axes are located in both cases in an almost identical position and enclose an angle of only 6.5°. The similarity of the transition pathways is clearly visible in the 2-D projections (Fig. 5) where they can be seen to connect nonoverlapping areas sampled by the two reference simulations, with the inner product of the first eigenvectors as high as 0.73. Our results indicate that i), the transitions are complete and convergence of the global conformational changes has been reached; and ii), the transitions occur along the same pathway.

The most significant changes in ϕ- and ψ-angles upon the conformational transition are almost completely confined within the hinge region defined by the DynDom analysis of the crystal structures (110–112, 259–261, 312–318). One could expect all ϕ- and ψ-angles of involved residues to reflect the hinge bending motion in a linear way, like hinges of a door. Although ϕ- and ψ-angles of several residues are highly correlated with the conformational change, many backbone angles are not, mainly caused by specific changes in the hydrogen-bonding pattern. The large flexibility of the backbone angles suggests that the hinge residues should be considered as a flexible rope-like element rather than a rigid hinge. The almost rigid domains could require some plasticity in the hinge, providing adaptability in response to possible strains. Several other systems will have to be studied to recognize whether this is a general feature of hinges or specific to MBP.

Hook-and-eye motif

Well-defined molecular rearrangements accompany the global conformational transition. A salt bridge between the side chain of Glu-111 in the hinge region and Lys-15 in the N-terminal domain, proximal to the reducing end of the bound sugar chain, forms and triggers a number of correlated transitions, shown in Fig. 7. The salt bridge between Glu-111 and Lys-15 operates as a latch (Fig. 6) that keeps the ligand-bound MBP in the closed conformation. Our holo-transition simulation shows that a salt bridge is formed during the domain closure pathway at the moment the side chain–side chain distance allows for it, at the expense of breaking a β-sheet hydrogen bond. Mutating Glu-111 to Lys abolished the sugar-binding capacity (15). This salt bridge has been identified previously in MBP (6,8) and similar salt bridges have been found in the glutamate-binding protein (49,50) and the ribose-binding protein (49,50), but its importance for function has to our knowledge not been recognized. The conformations of Glu-111 and Lys-15 are similar in both the completely open and the closed structure, whereas functionally relevant structural changes occur on the domain motion

pathway, guiding domain closure. This salt bridge locks the ligand-bound MBP in a semiclosed conformation. A force toward the completion of substrate capture is exerted by the disrupted hydrogen bond between Glu-111 and Gly-260 that can only be restored at complete domain closure. The local three-step mechanism can be recognized on the global scale. The time points at which these events occur correlate with distinct regions found in the 2-D eigenvector projection (Fig. 7 *E*)—the open, the intermediate, and a closed conformation—although the time points of the local changes anticipate the global structural transition by a small extent. This motion cannot directly be related to sugar transport, because in our system the $MalFGK_2$ transporter is absent, but our results indicate that once the substrate has left the binding site, MBP is more stable in the open conformation in line with a vanadate-trapped intermediate state of sugar transport (51). It is interesting to note in the context of the proposed hook-and-eye motif, that the MBP mutants Gly-13Asp and Asp-14Tyr at the edge of the binding pocket, next to Lys-15, have been shown to inhibit maltose transport by interacting with wild-type transporter in a nonproductive manner (16) and to allele specifically restore maltose transport in $MalFGK_2$ mutant strains (15), whereas a Tyr-155His mutant is indicated to affect transport by indirect effect. This suggests a potential relation between the hook-and-eye motif identified in our study and the stability of the closed conformation and sugar transport.

Chemotaxis and transport

The ligand-bound closed MBP is required to trigger the formation of the strong binding complex of MBP with the maltose ABC transporter $MalFGK_2$ that subsequently enables sugar transport (51,52). The change in relative distance between the two domains seems to be important for transport. Of particular relevance are the loops in the N-terminal domain that contact the ligand as well as helix II and Trp-210 on the C-terminal domain (Fig. 8 *A*). The suppressor mutants Gly-13Asp and Asp-14Tyr show stronger binding to the transporter compared to the wild-type MBP. These interactions could potentially represent a strain on the closed MBP that could disrupt the salt bridge in the hook-and-eye motif and destabilize the closed conformation.

Binding of the ligand-bound MBP to Tar induces signal transduction that ultimately affects the activity of the *Escherichia coli* flagella and therefore the motion of the bacteria toward nutrients (53). The surface area of MBP relevant for chemotaxis has been identified by mutation analysis (16,51,54–57) and is confined in the region of helix II and helix III on the N-terminal domain, and in the last two helices of the C-terminal domain. The relative orientation of the relevant helices differs widely between the open and the closed states. A docking study (57) indicated that these key regions have the correct relative orientation only in the closed conformation (57,58) (see Fig. 8 *B*).

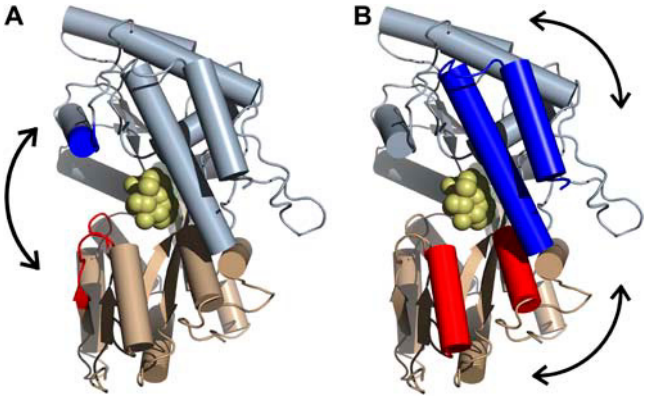

FIGURE 8 (*A*) Residues involved in transport. (*B*) Helices involved in chemotaxis. The functionally important residues are highlighted in red and blue. The arrows symbolize the changes of these elements by the conformational transition. The ligand is shown in yellow. The figures were prepared with PyMOL (69).

The chemotaxis receptor Tar and the ABC transporter $MalFGK_2$ use the structural differences from the large conformational changes of MBP as a signal to recognize the presence of oligosaccharides. This interpretation requires the apo MBP to be predominantly in the open conformation to avoid the stimulation of an incorrect signal. Several open ligand-bound structures of periplasmic binding proteins have been determined, a closed apo structure of the glucose/galactose-binding protein (59) has been crystallized, and antibody binding studies have demonstrated that the apo form of histidine-binding protein can adopt both conformations (60). Based on this data, it has been hypothesized that periplasmic binding proteins could exist in an equilibrium between open and closed conformations in both binding states (9) following the Monod-Wyman-Changeux model (61). Our simulations indicate that MBP is predominantly in the open conformation when ligand-free and in the closed state when ligand-bound, thereby resembling the Koshland-Nemethy-Filmer (62) induced fit model. This finding is supported by NMR experiments (63) that determined the solution structure of MBP. These studies illustrate that apo MBP is in the open state and the ligand-bound MBP is in the closed state. The NMR experiments suggests that the apo open state of MBP is stabilized by 31.4 kJ/mol in the ligand-free form compared to the closed form, whereas the closed state is stabilized by 35.1 $\pm$ 0.8 kJ/mol relative to the open state in the ligand-bound form (64). Although we cannot calculate a free energy difference from our simulations, we tried to estimate the effect of a change in hydrophobic solvent accessible surface area. We calculate a decrease (averaged over the last 10 ns) in the hydrophobic solvent accessible surface area (65) between the closed and the open conformation of MBP (probe radius 0.14 nm) of 1.4 $\pm$ 0.2 nm^2 upon domain opening. This change in area, using a simple estimate of the free energy cost of exposing hydrophobic surface (66), corresponds to a free energy

difference of ~9 kJ/mol. This is a significant contribution to the overall free energy change promoting opening in the apo form. In the presence of the ligand, the total change in solvent exposed hydrophobic surface area is a decrease of 2.2 ± 0.3 nm^2 upon ligand binding and domain closure, corresponding to a contribution of ~17 kJ/mol to the solvation free energy. Electrostatic interactions between the two domains and the ligand as well as entropic terms might be additional factors, but these are difficult to estimate from the simulations. Finally we can compare our results to the conformational changes detected in solution by SAXS experiments (42). The overall agreement is good (see Fig. 3). The shape of the $P(r)$ function and the effect of sugar binding are well reproduced by the simulations. Ligand-free MBP is in the elongated open conformation and becomes more compact upon ligand-binding, supporting the view of a predominantly open apo form and a closed holo state of MBP.

CONCLUSIONS

In this study we show that large conformational changes (~30° rotation) induced by changes in the ligand binding state can be successfully investigated by MD simulations on a timescale of 30 ns without the need of an additional bias. The strength of the simulation approach is evident in the convergence of both the apo and the holo simulations as well as in the characterization of the hook-and-eye motif that shows highly correlated local structural changes with functionally important global effects along the transition pathway. The proximity of Lys-15 of the hook-and-eye motif to residue Gly-13 and Asp-14, that have been shown to prominently interact with MalG, points toward an important role of this motif in substrate transport.

SUPPLEMENTARY MATERIAL

An online supplement to this article can be found by visiting BJ Online at http://www.biophysj.org.

This work was supported by the Canadian Institutes of Health Research (CIHR) and the Alberta Synchrotron Institute. D.P.T. is an Alberta Heritage Foundation for Medical Research (AHFMR) Senior Scholar, a CIHR New Investigator, and a Sloan Foundation Fellow. H.G.V. is an AHFMR Scientist. We acknowledge computational support from WestGrid.

REFERENCES

1. Higgins, C. F. 1992. ABC transporters—from microorganisms to man. *Annu. Rev. Cell Biol.* 8:67–113.
2. Stock, J. B., and M. G. Surette. 1996. Chemotaxis. *In Escherichia coli* and Salmonella: Cellular and Molecular Biology, 2nd ed. F. C. Neidhardt, editor. ASM Press, Washington, D.C. 1103–1129.
3. Quiocho, F. A., and P. S. Ledvina. 1996. Atomic structure and specificity of bacterial periplasmic receptors for active transport and chemotaxis: variation of common themes. *Mol. Microbiol.* 20:17–25.
4. Sugiyama, S., Y. Matsuo, K. Maenaka, D. G. Vassylyev, M. Matsushima, K. Kashiwagi, K. Igarashi, and K. Morikawa. 1996. The 1.8-Å x-ray structure of the *Escherichia coli* PotD protein complexed with spermidine and the mechanism of polyamine binding. *Protein Sci.* 5:1984–1990.
5. Krewulak, K. D., R. S. Peacock, and H. J. Vogel. 2004. Periplasmic binding proteins involved in bacterial iron uptake. *In* Iron Transport in Bacteria. J. H. Corsa, A. R. Mey, and S. M. Payne, editors. ASM Press, Washington, D.C. 118–129.
6. Spurlino, J. C., G. Y. Lu, and F. A. Quiocho. 1991. The 2.3-Å resolution structure of the maltose-binding or maltodextrin-binding protein, a primary receptor of bacterial active-transport and chemotaxis. *J. Biol. Chem.* 266:5202–5219.
7. Fukami-Kobayashi, K., Y. Tateno, and K. Nishikawa. 1999. Domain dislocation: a change of core structure in periplasmic binding proteins in their evolutionary history. *J. Mol. Biol.* 286:279–290.
8. Sharff, A. J., L. E. Rodseth, J. C. Spurlino, and F. A. Quiocho. 1992. Crystallographic evidence of a large ligand-induced hinge-twist motion between the 2 domains of the maltodextrin binding-protein involved in active-transport and chemotaxis. *Biochemistry.* 31:10657–10663.
9. Boos, W., and J. M. Lucht. 1996. Periplasmic Binding Protein-Dependent ABC Transporters. *In Escherichia coli* and *Salmonella*: Cellular And Molecular Biology, 2nd ed. F. C. Neidhardt, editor. ASM Press, Washington, D.C. 1149–1209.
10. Boos, W., and H. Shuman. 1998. Maltose/maltodextrin system of *Escherichia coli*: transport, metabolism, and regulation. *Microbiol. Mol. Biol. Rev.* 62:204–229.
11. Quiocho, F. A., J. C. Spurlino, and L. E. Rodseth. 1997. Extensive features of tight oligosaccharide binding revealed in high-resolution structures of the maltodextrin transport/chemosensory receptor. *Structure.* 5:997–1015.
12. Kellermann, O., and S. Szmelcman. 1974. Active transportation of maltose in *Escherichia coli* K-12. Involvement of a perplasmic maltose-binding protein. *Eur. J. Biochem.* 47:139–149.
13. Szmelcman, S., M. Schwartz, T. J. Silhavy, and W. Boos. 1976. Maltose transport in *Escherichia coli*-K12—Comparison of transport kinetics in wild-type and lambda-resistant mutants with dissociation-constants of maltose-binding protein as measured by fluorescence quenching. *Eur. J. Biochem.* 65:13–19.
14. Treptow, N. A., and H. A. Shuman. 1985. Genetic-evidence for substrate and periplasmic-binding-protein recognition by the malf and malg proteins, cytoplasmic membrane-components of the *Escherichia coli* maltose transport-system. *J. Bacteriol.* 163:654–660.
15. Treptow, N. A., and H. A. Shuman. 1988. Allele-specific male mutations that restore interactions between maltose-binding protein and the inner-membrane components of the maltose transport-system. *J. Mol. Biol.* 202:809–822.
16. Hor, L. I., and H. A. Shuman. 1993. Genetic-analysis of periplasmic binding-protein dependent transport in *Escherichia coli*—each lobe of maltose-binding protein interacts with a different subunit of the MalFGK(2) membrane-transport complex. *J. Mol. Biol.* 233: 659–670.
17. Pang, A., Y. Arinaminpathy, M. S. P. Sansom, and P. C. Biggin. 2003. Interdomain dynamics and ligand binding: molecular dynamics simulations of glutamine binding protein. *FEBS Lett.* 550:168–174.
18. Arinaminpathy, Y., M. S. Sansom, and P. C. Biggin. 2002. Molecular dynamics simulations of the ligand-binding domain of the ionotropic glutamate receptor GluR2. *Biophys. J.* 82:676–683.
19. Roccatano, D., A. E. Mark, and S. Hayward. 2001. Investigation of the mechanism of domain closure in citrate synthase by molecular dynamics simulation. *J. Mol. Biol.* 310:1039–1053.
20. Daidone, I., D. Roccatano, and S. Hayward. 2004. Investigating the accessibility of the closed domain conformation of citrate synthase using essential dynamics sampling. *J. Mol. Biol.* 339:515–525.
21. Tirion, M. M. 1996. Large amplitude elastic motions in proteins from a single-parameter, atomic analysis. *Phys. Rev. Lett.* 77:1905–1908.

22. Tama, F., and Y. H. Sanejouand. 2001. Conformational change of proteins arising from normal mode calculations. *Protein Eng.* 14:1–6.

23. Kitao, A., and N. Go. 1991. Conformational dynamics of polypeptides and proteins in the dihedral angle space and in the cartesian coordinate space—normal mode analysis of deca-alanine. *J. Comput. Chem.* 12: 359–368.

24. Echols, N., D. Milburn, and M. Gerstein. 2003. MolMovDB: analysis and visualization of conformational change and structural flexibility. *Nucleic Acids Res.* 31:478–482.

25. Miller, D. M., J. S. Olson, J. W. Pflugrath, and F. A. Quiocho. 1983. Rates of ligand-binding to periplasmic proteins involved in bacterial transport and chemotaxis. *J. Biol. Chem.* 258:3665–3672.

26. Rubin, S. M., S. Y. Lee, E. J. Ruiz, A. Pines, and D. E. Wemmer. 2002. Detection and characterization of xenon-binding sites in proteins by 129Xe NMR spectroscopy. *J. Mol. Biol.* 322:425–440.

27. Biotech Validation Suite for Protein Structures. http://biotech.ebi.ac.uk:8400.

28. Duan, X., and F. A. Quiocho. 2002. Structural evidence for a dominant role of nonpolar interactions in the binding of a transport/chemosensory receptor to its highly polar ligands. *Biochemistry.* 41:706–712.

29. Lindahl, E., B. Hess, and D. van der Spoel. 2001. GROMACS 3.0: a package for molecular simulation and trajectory analysis. *J. Mol. Model. (Online).* 7:306–317.

30. Berendsen, H. J. C., D. Vanderspoel, and R. Vandrunen. 1995. GROMACS—a message-passing parallel molecular-dynamics implementation. *Comput. Phys. Commun.* 91:43–56.

31. Scott, W. R. P., P. H. Hunenberger, I. G. Tironi, A. E. Mark, S. R. Billeter, J. Fennen, A. E. Torda, T. Huber, P. Kruger, and W. F. van Gunsteren. 1999. The GROMOS biomolecular simulation program package. *J. Phys. Chem. A.* 103:3596–3607.

32. Berendsen, H. J. C., J. P. M. Postma, W. F. van Gunsteren, and J. Hermans. 1981. Interaction models for water in relation to protein hydration. *In* Intermolecular Forces. B. Pullman, editor. Reidel, Dordrecht, The Netherlands. 331–342.

33. Berendsen, H. J. C., J. P. M. Postma, W. F. van Gunsteren, A. DiNola, and J. R. Haak. 1984. Molecular dynamics with coupling to an external bath. *J. Chem. Phys.* 81:3684–3689.

34. Essmann, U., L. Perera, M. L. Berkowitz, T. Darden, H. Lee, and L. G. Pedersen. 1995. A smooth particle mesh Ewald method. *J. Chem. Phys.* 103:8577–8593.

35. Darden, T., D. York, and L. Pedersen. 1993. Particle mesh Ewald—an N.Log(N) method for Ewald sums in large systems. *J. Chem. Phys.* 98:10089–10092.

36. Hess, B., H. Bekker, H. J. C. Berendsen, and J. G. E. M. Fraaije. 1997. LINCS: a linear constraint solver for molecular simulations. *J. Comput. Chem.* 18:1463–1472.

37. Miyamoto, S., and P. A. Kollman. 1992. SETTLE. *J. Comput. Chem.* 13:952–962.

38. Feenstra, K. A., B. Hess, and H. J. C. Berendsen. 1999. Improving efficiency of large time-scale molecular dynamics simulations of hydrogen-rich systems. *J. Comput. Chem.* 20:786–798.

39. Amadei, A., A. B. M. Linssen, and H. J. C. Berendsen. 1993. Essential dynamics of proteins. *Proteins.* 17:412–425.

40. Hayward, S., and H. J. C. Berendsen. 1998. Systematic analysis of domain motions in proteins from conformational change: New results on citrate synthase and T4 lysozyme. *Proteins.* 30:144–154.

41. Hayward, S., and R. A. Lee. 2002. Improvements in the analysis of domain motions in proteins from conformational change: DynDom version 1.50. *J. Mol. Graph. Model.* 21:181–183.

42. Shilton, B. H., M. M. Flocco, M. Nilsson, and S. L. Mowbray. 1996. Conformational changes of three periplasmic receptors for bacterial chemotaxis and transport: The maltose-, glucose/galactose- and ribose-binding proteins. *J. Mol. Biol.* 264:350–363.

43. Merzel, F., and J. C. Smith. 2002. Is the first hydration shell of lysozyme of higher density than bulk water? *Proc. Natl. Acad. Sci. USA.* 99:5378–5383.

44. Svergun, D. I., S. Richard, M. H. J. Koch, Z. Sayers, S. Kuprin, and G. Zaccai. 1998. Protein hydration in solution: experimental observation by x-ray and neutron scattering. *Proc. Natl. Acad. Sci. USA.* 95:2267–2272.

45. Clarke, T. E., S. Y. Ku, D. R. Dougan, H. J. Vogel, and L. W. Tari. 2000. The structure of the ferric siderophore binding protein FhuD complexed with gallichrome. *Nat. Struct. Biol.* 7:287–291.

46. Borths, E. L., K. P. Locher, A. T. Lee, and D. C. Rees. 2002. The structure of *Escherichia coli* BtuF and binding to its cognate ATP binding cassette transporter. *Proc. Natl. Acad. Sci. USA.* 99:16642–16647.

47. Karpowich, N. K., H. H. Huang, P. C. Smith, and J. F. Hunt. 2003. Crystal structures of the BtuF periplasmic-binding protein for vitamin B12 suggest a functionally important reduction in protein mobility upon ligand binding. *J. Biol. Chem.* 278:8429–8434.

48. Krewulak, K. D., C. M. Shepherd, and H. J. Vogel. 2005. Molecular dynamics simulations of the periplasmic ferric-hydroxamate binding protein FhuD. *Biometals.* 8:375–386.

49. Bjorkman, A. J., and S. L. Mowbray. 1998. Multiple open forms of ribose-binding protein trace the path of its conformational change. *J. Mol. Biol.* 279:651–664.

50. Sun, Y. J., J. Rose, B. C. Wang, and C. D. Hsiao. 1998. The structure of glutamine-binding protein complexed with glutamine at 1.94 angstrom resolution: comparisons with other amino acid binding proteins. *J. Mol. Biol.* 278:219–229.

51. Austermuhle, M. I., J. A. Hall, C. S. Klug, and A. L. Davidson. 2004. Maltose-binding protein is open in the catalytic transition state for ATP hydrolysis during maltose transport. *J. Biol. Chem.* 279:28243–28250.

52. Zhang, Y. H., D. E. Mannering, A. L. Davidson, N. H. Yao, and M. D. Manson. 1996. Maltose-binding protein containing an interdomain disulfide bridge confers a dominant-negative phenotype for transport and chemotaxis. *J. Biol. Chem.* 271:17881–17889.

53. Koiwai, O., and H. Hayashi. 1979. Studies on bacterial chemotaxis.4. Interaction of maltose receptor with a membrane-bound chemosensing component. *J. Biochem. (Tokyo).* 86:27–34.

54. Manson, M. D., and M. Kossmann. 1986. Mutations in tar suppress defects in maltose chemotaxis caused by specific male mutations. *J. Bacteriol.* 165:34–40.

55. Kossmann, M., C. Wolff, and M. D. Manson. 1988. Maltose chemoreceptor of *Escherichia coli*—interaction of maltose-binding protein and the tar signal transducer. *J. Bacteriol.* 170:4516–4521.

56. Gardina, P., C. Conway, M. Kossman, and M. Manson. 1992. Aspartate and maltose-binding protein interact with adjacent sites in the tar chemotactic signal transducer of *Escherichia coli*. *J. Bacteriol.* 174:1528–1536.

57. Zhang, Y. H., P. J. Gardina, A. S. Kuebler, H. S. Kang, J. A. Christopher, and M. D. Manson. 1999. Model of maltose-binding protein/chemoreceptor complex supports intrasubunit signaling mechanism. *Proc. Natl. Acad. Sci. USA.* 96:939–944.

58. Milburn, M. V., G. G. Prive, D. L. Milligan, W. G. Scott, J. Yeh, J. Jancarik, D. E. Koshland, and S. H. Kim. 1991. 3-dimensional structures of the ligand-binding domain of the bacterial aspartate receptor with and without a ligand. *Science.* 254:1342–1347.

59. Flocco, M. M., and S. L. Mowbray. 1994. The 1.9 Angstrom x-ray structure of a closed unliganded form of the periplasmic glucose/galactose receptor from *Salmonella typhimurium*. *J. Biol. Chem.* 269: 8931–8936.

60. Wolf, A., E. W. Shaw, K. Nikaido, and G. F. L. Ames. 1994. The histidine-binding protein undergoes conformational-changes in the absence of ligand as analyzed with conformation-specific monoclonal-antibodies. *J. Biol. Chem.* 269:23051–23058.

61. Monod, J., J. Wyman, and J. P. Changeux. 1965. On the nature of allosteric transitions: a plausible model. *J. Mol. Biol.* 12:88–118.

62. Koshland, D. E., Jr., G. Nemethy, and D. Filmer. 1966. Comparison of experimental binding data and theoretical models in proteins containing subunits. *Biochemistry.* 5:365–385.

63. Evenas, J., V. Tugarinov, N. R. Skrynnikov, N. K. Goto, R. Muhandiram, and L. E. Kay. 2001. Ligand-induced structural changes to maltodextrin-binding protein as studied by solution NMR spectroscopy. *J. Mol. Biol.* 309:961–974.

64. Millet, O., R. P. Hudson, and L. E. Kay. 2003. The energetic cost of domain reorientation in maltose-binding protein as studied by NMR and fluorescence spectroscopy. *Proc. Natl. Acad. Sci. USA*. 100: 12700–12705.

65. Eisenhaber, F., P. Lijnzaad, P. Argos, C. Sander, and M. Scharf. 1995. The double cubic lattice method—efficient approaches to numerical-integration of surface-area and volume and to dot surface contouring of molecular assemblies. *J. Comput. Chem.* 16:273–284.

66. Eisenberg, D., and A. D. Mclachlan. 1986. Solvation energy in protein folding and binding. *Nature*. 319:199–203.

67. Kraulis, P. J. 1991. MolScript—a program to produce both detailed and schematic plots of protein structures. *J. Appl. Crystallogr.* 24:946–950.

68. Merritt, E. A., and D. J. Bacon. 1997. Raster3D: photorealistic molecular graphics. *Methods Enzymol.* 277:505–524.

69. PyMOL. DeLano Scientific. http://pymol.sourceforge.net